THE JOURNAL OF PHYSICAL CHEMISTRY C

Article

pubs.acs.org/JPCC

Surface Phase Transition in Anomalous Fluid in Nanoconfinement

José Rafael Bordin,*[,†,§] Leandro B. Krott,*[,‡] and Marcia C. Barbosa*[,‡]

[†]Campus Caçapava do Sul, Universidade Federal do Pampa, Av. Pedro Anunciação, s/no, CEP 96570-000, Caçapava do Sul, RS Brazil

[‡]Instituto de Física, Universidade Federal do Rio Grande do Sul, Caixa Postal 15051, CEP 91501-970, Porto Alegre, RS Brazil

[§]Departamento de Física, Instituto de Física e Matemática, Universidade Federal de Pelotas, Caixa Postal 354, CEP 96010-900, Pelotas, RS Brazil

ABSTRACT: We explore by molecular dynamic simulations the thermodynamical behavior of an anomalous fluid confined inside rigid and flexible nanopores. The fluid is modeled by a two length scale potential. In the bulk, this system exhibits the density and diffusion anomalous behavior observed in liquid water. We show that the anomalous fluid confined inside rigid and flexible nanopores forms layers. As the volume of the nanopore is decreased the rigid surface exhibits three consecutive first-order phase transitions associated with the change in the number of layers. These phase transitions are not present for flexible confinement. Our results indicate that the nature of confinement is relevant for the properties of the confined liquid, which suggests that confinement in carbon nanotubes should be quite different from confinement in biological channels.

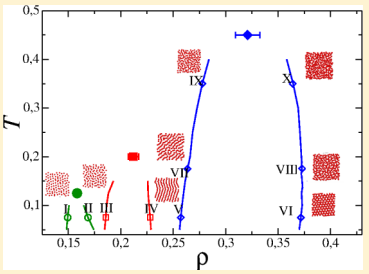

1. INTRODUCTION

Most liquids contract on cooling and diffuse faster as the density is decreased. This is not the case of the anomalous liquids, in which the density exhibits a maximum at constant pressure and the diffusion coefficient increases under compression.[1] These anomalous fluids include water,[2−4] Te,[5] Ga, Bi,[6] Si,[7,8] $Ge_{15}Te_{85}$,[9] liquid metals,[10] and graphite.[11] Computer simulations for silica,[12−14] silicon,[15] and BeF_2[12] also show the presence of thermodynamic anomalies.[4] In addition to the presence of a maximum of density in constant pressure, silica,[13−16] silicon,[17] and water[18,19] exhibit a maximum in the diffusion coefficient at constant temperature.

Classical all-atom models such as SPC/E,[20] TIP4P-2005,[21] and TIP5P[22] for water, sW[23] for silicon, or BKS[24] for silica have been employed to reproduce quantitatively these anomalous properties of these materials. However, coarse-grained potentials are an interesting tool able to identify the common structural property in these fluids that make them anomalous. The effective potentials derived in these coarse-grained models are analytically more tractable and also computationally less expensive, which allows for studying a very large systems and complex mixtures. Several effective models have been proposed.[23−35] They reproduce the thermodynamic, structural, and dynamic anomalies present in water and in other anomalous liquids. The common ingredient in these potentials is that the particle−particle interaction is modeled through core-softened potentials formed by two length scales, one repulsive shoulder, and an attractive well.[29,36−38] This competition leads to the density and diffusion anomalies.

In addition to the bulk properties, nanoconfinement of anomalous liquids has been attracting attention not only due to its applications but also due to the new physics observed in these systems.[39−41] Fluids confined in carbon nanotube exhibit the formation of layers, crystallization of the contact layer,[42,43] and a superflow not present in macroscopic confinement.[44−46]

In the particular case of water confined in nanopores, the pore size has significant influence on the freezing and melting temperatures of water.[47−50] The crystallization in these systems is not uniform, and the confined ice shows different characteristics when compared with the bulk ice.[51] Hydrophobic[46,52−54] confinements also induce different effects in the layering, density, and flow of water.

Atomistic studies of nanoconfinement of water show another property: confined systems exhibit a phase transition not observed in the bulk system. SPC/E model confined between atomically smooth plates[56,57] and TIP4P water inside nanotubes[58] shows a first-order phase transition between a bilayer liquid (or ice) and a trilayer heterogeneous fluid. These studies, however, have been restricted to rigid nanotubes. The flexibility of the nanochannel[44,45] and of biological ionic channels[59−62] shows properties different from the behavior observed in confinement by rigid walls. These studies, however, do not highlight the physical reason behind the differences between rigid and flexible confinement.

Acknowledging that coarse-graining potentials would be a suitable tool to test how the flexibility would affect the properties of confined anomalous liquids. Recently it was shown that the density and diffusion anomalies disappear as the channel or nanopore become flexible.[63]

We explore the differences in the layering and in the surface phase transitions for anomalous fluids confined by both rigid and flexible nanotubes. We show that the surface crystallization observed in rigid carbon nanotubes should not be expected in flexibly biological channels. The fluid is modeled using a two length scale potential. This coarse-grained potential exhibits the thermodynamic, dynamic, and structural anomalous behavior

Received: January 29, 2014
Revised: April 10, 2014
Published: April 18, 2014

   dx.doi.org/10.1021/jp5010506 | J. Phys. Chem. C 2014, 118, 9497−9506

observed in anomalous fluids in bulk[29,36] and in confinement.[63−67] The formation of layers and its relation to the first-order phase transition are analyzed. The paper is organized as follows: in Section 2 we introduce the model and describe the methods and simulation details; the results are given in Section 3; and in Section 4 we present our conclusions.

2. MODEL AND THE SIMULATION METHODOLOGY

The fluid is modeled as spherical-symmetric particles, with diameter σ and mass m. The particles interact through the 3-D core-softened potential[29]

$$\frac{U(r_{ij})}{\varepsilon} = 4\left[\left(\frac{\sigma}{r_{ij}}\right)^{12} - \left(\frac{\sigma}{r_{ij}}\right)^{6}\right] + u_0 \exp\left[-\frac{1}{c_0^2}\left(\frac{r_{ij} - r_0}{\sigma}\right)^2\right] \tag{1}$$

where $r_{ij} = |\vec{r}_i - \vec{r}_j|$ is the distance between two fluid particles i and j. This potential has two contributions. The first parcel is the standard 12−6 Lennard-Jones (LJ) potential,[68] and the second term is a Gaussian centered at $r_0/\sigma = 0.7$, with depth $u_0 = 5.0$ and width $c_0 = 1.0$. With these parameters, eq 1 represents a two length scale potential, with one scale at $r_{ij} \approx 1.2\sigma$, where the force has a local minimum, and the other scale at $r_{ij} \approx 2\sigma$, where the fraction of imaginary modes has a local minimum,[69] as shown in Figure 1. We should address that the attractive well

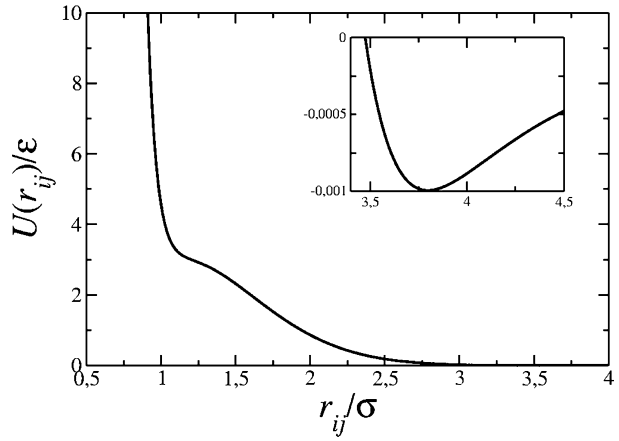

Figure 1. Interaction potential between anomalous fluid particles pair as a function of their separation. Inset: zoom over the small attractive part of the interaction.

shown in the inset of Figure 1 is negligible. The fluid−fluid interaction, eq 1, has a cutoff radius $r_{cut}/\sigma = 3.5$. Despite the mathematical simplicity of the model, this fluid exhibits the thermodynamic, dynamic, and structural anomalies present in bulk water[29,36] and a water-like behavior when confined between plates[63−65] or inside hydrophobic nanotubes.[66,67]

The nanopore was modeled using two flat parallel walls, with fixed dimension $L \times L$, where $L = 20\sigma$, separated by a distance L_z. In Figure 2 we show the snapshot of the system for two distinct configurations, one with a large L_z, where the fluid shows a bulk-like behavior, and the other a highly confined fluid. The fluid−wall interaction is purely repulsive and was represented by the Weeks−Chandler−Andersen (WCA)[70] potential

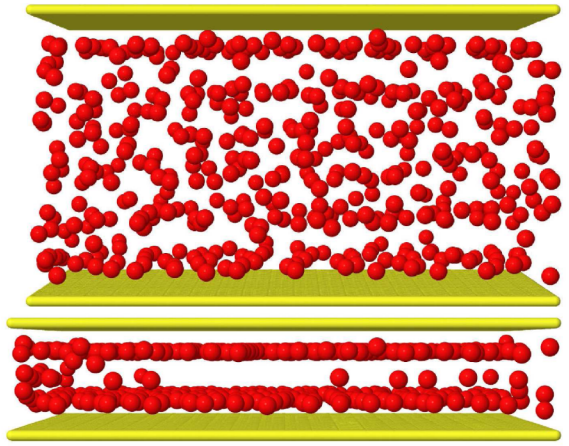

Figure 2. Snapshot of the simulation box for system for large (up) and narrow (down) nanopores.

$$U^{\mathrm{WCA}}(z_{ij}) = \begin{cases} U_{\mathrm{LJ}}(z_{ij}) - U_{\mathrm{LJ}}(z_c), & z_{ij} \le z_c \\ 0, & z_{ij} > z_c \end{cases} \tag{2}$$

Here U_{LJ} is the standard 12−6 LJ potential, included in the first term of eq 1, and $z_c = 2^{1/6}\sigma$ is the cutoff for the WCA potential. Also, the term z_{ij} measures the distance between the wall at j position and the z-coordinate of the fluid particle i.

Two distinct scenarios were studied: rigid and flexible walls. In the first case, the nanopore wall positions were fixed and standard *NVT* molecular dynamic simulations were performed. The temperature control was obtained with the Nosè−Hoover thermostat, with a coupling parameter $Q = 2.0$. The pressure in the z direction, p_z, was computed by the virial expression in the direction of the confinement (z),[71] namely

$$p_z = \rho k_b T + \frac{1}{V}\langle W_t \rangle \tag{3}$$

where

$$\langle W_t \rangle = -\sum_{1}^{N}\sum_{j>1}^{N} \frac{z_{ij}^2}{r_{ij}}\frac{\partial U}{\partial r}$$

and $U(r_{ij})$ is the interaction potential between two particles separated by a distance r_{ij} and z_{ij} is the z component of the distance.

In a second scenario, flexible walls were studied. In this case, MD simulations were performed at constant number of particles and perpendicular pressure and temperature (Np_zT ensemble). The pressure was fixed using the Lupowski and van Smol method.[72] The walls had translational freedom in the z direction, acting like a piston in the fluid, and a constant force controls the pressure applied in the confined direction. In this scenario, the resulting force in a fluid particle is given by

$$\vec{F}_R = -\vec{\nabla}U + \vec{F}_{iwA}(\vec{r}_{iA}) + \vec{F}_{iwB}(\vec{r}_{iB}) \tag{4}$$

where $\vec{F}_{iwA(B)}$ indicates the interaction between the particle i and the piston $A(B)$. Once the walls are nonrigid and time-dependent, we have to solve the equations of motion for A and B

$$m_w \vec{a}_A = p_z S_w \vec{n}_A - \sum_{i=1}^{N} \vec{F}_{iwA}(\vec{r}_{iA}) \tag{5}$$

dx.doi.org/10.1021/jp5010506 | J. Phys. Chem. C 2014, 118, 9497−9506

and

$$m_w \vec{a}_B = p_z S_w \vec{n}_B - \sum_{i=1}^{N} \vec{F}_{iwB}(\vec{r}_{iB}) \quad (6)$$

respectively, where m_w is the piston mass, p_z is the applied pressure in the system, S_w is the piston area, and $\vec{n}_A$ is an unitary vector in positive z direction, while $\vec{n}_B$ is a negative unitary vector. Both pistons (A and B) have mass $m_w = m$, width σ, and area equal to $S_w = L^2$.

For the rigid nanopore system, the temperature was varied from $k_BT/\varepsilon = 0.05$ to $k_BT/\varepsilon = 1.00$ and the plate separation was varied from $L_z = 4.00\sigma$ to $L_z = 10.00\sigma$, while for systems with flexible nanopores the temperature was varied from $k_BT/\varepsilon = 0.10$ to $k_BT/\varepsilon = 1.00$ and the perpendicular pressure was varied from $p_z\sigma^3/\varepsilon = 0.075$ to $p_z\sigma^3/\varepsilon = 6.00$. In both cases the simulations where performed with $N = 500$ particles. Because of the excluded volume originated by the nanopore−fluid interaction, the distance $L_z\sigma$ between them needs to be corrected to an effective distance,[73,74] $L_{ze}\sigma$, that can be approached by $L_{ze}/\sigma \approx L_z/\sigma - 1$. Consequently, the effective density will be $\rho_e\sigma^3 = N/(L_{ze}L^2)$. For flexible nanopores, considering the fluctuation of the walls, the effective distance will oscillate around an average value $\langle L_{ze}/\sigma\rangle$, and the average density will be $\rho_e\sigma^3 = N/\langle L_{ze}\rangle L^2$. Also, it is important to reinforce that N is fixed for all simulations and the distinct values for density are obtained by the variation in the plates separation, L_z. Standard periodic boundary conditions were applied in the nonconfined directions. Five independent runs were performed to evaluate the properties of the confined fluid. Each individual simulation consists of 1×10^6 equilibration steps and 3×10^6 steps for production, with a time step $\delta t = 0.0025$ in LJ units.

To define the fluid characteristics in contact with the nanopore walls, the structure of the fluid contact layer was analyzed using the radial distribution function $g_{\parallel}(r_{xy})$, defined as

$$g_{\parallel}(r_{xy}) \equiv \frac{1}{\rho^2 V} \sum_{i\neq j} \delta(r - r_{ij})[\theta(|z_i - z_j|) - \theta(|z_i - z_j| - \delta z)] \quad (7)$$

where the Heaviside function $\theta(x)$ restricts the sum of particle pair in a slab of thickness $\delta z = 1.0$ close to the wall.

Also, to verify the fluid mobility, we calculate the lateral mean square displacement (MSD)

$$\langle[\vec{r}_{\parallel}(t) - \vec{r}_{\parallel}(t_0)]^2\rangle = \langle\Delta\vec{r}_{\parallel}(t)^2\rangle = 4Dt^{\alpha} \quad (8)$$

where $\vec{r}_{\parallel}(t_0) = (x(t_0)^2 + y(t_0)^2)^{1/2}$ and $\vec{r}_{\parallel}(t) = (x(t)^2 + y(t)^2)^{1/2}$ denote the parallel coordinate of the confined fluid molecule at a time t_0 and at a later time t, respectively.

The physical quantities will be depict in the standard LJ units[68]

$$r^* \equiv \frac{r}{\sigma},\ \rho^* \equiv \rho\sigma^3,\ \text{and } t^* \equiv t\left(\frac{\varepsilon}{m\sigma^2}\right)^{1/2} \quad (9)$$

for distance, density of particles and time, respectively, and

$$p^* \equiv \frac{p\sigma^3}{\varepsilon} \text{ and } T^* \equiv \frac{k_BT}{\varepsilon} \quad (10)$$

for the pressure and temperature, respectively. Because all physical quantities are defined in reduced LJ units in this paper, the * will be omitted to simplify the discussion of our results.

In the simulations with flexible nanopores, the mean variation in the system size induced by the wall fluctuations is smaller than 2%. Data errors smaller than the data points are not shown.

3. RESULTS AND DISCUSSION

To understand the thermodynamical properties of the anomalous fluid under confinement, the $p_z \times \rho$ phase diagram

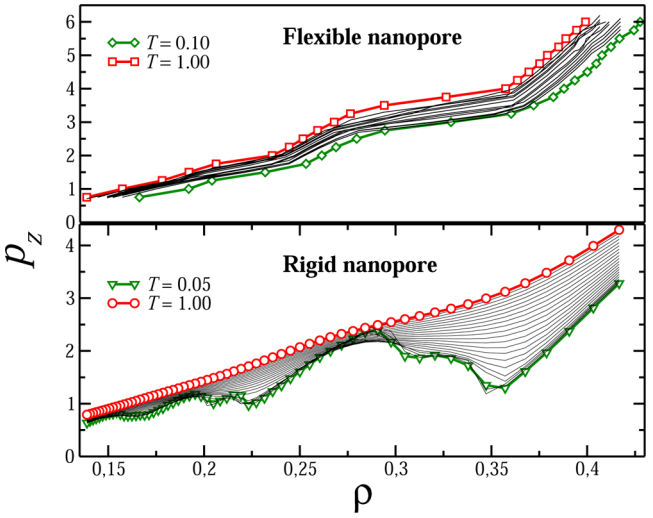

Figure 3. Pressure in the confined direction as a function of the fluid density for flexible and rigid nanopores for several values of temperature. For simplicity, only the higher and lower values of T for the isotherms are detached. A nonmonotonic behavior was observed when the anomalous fluid is confined inside rigid nanopores. All quantities are in reduced units.

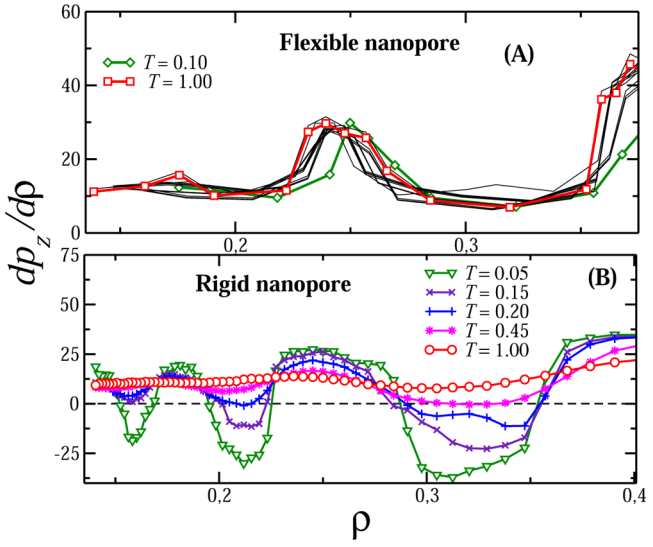

Figure 4. Pressure derivative versus density for different isotherms for (A) flexible or (B) rigid nanopores. In the rigid case, the inflection in $dp_z/d\rho = 0$ indicates the presence of a first-order phase transition.

is analyzed for the cases with flexible or rigid nanopores. Figure 3 illustrates the pressure in the confined direction versus density phase diagram for various temperatures. For the flexible nanopores, all isotherms show a monotonic behavior. This suggests that while the fluid between the plates changes its configuration between different layer arrangements of the wall

dx.doi.org/10.1021/jp5010506 | J. Phys. Chem. C 2014, 118, 9497−9506

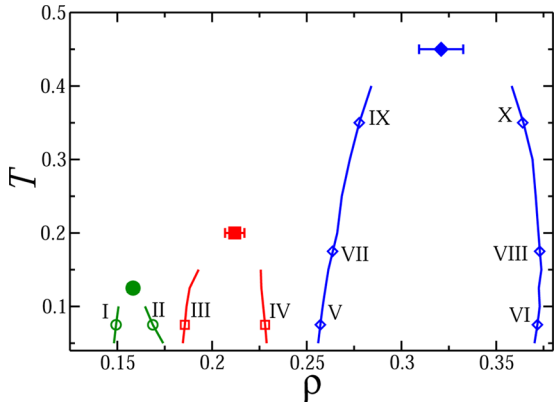

Figure 5. Temperature versus density phase diagram for the three coexistence regions and critical points: (T_{c1} = 0.125, $p_{z,c1}$ = 0.782, ρ_{c1} = 0.1583) (sphere), (T_{c2} = 0.2, $p_{z,c2}$ = 1.1704, ρ_{c2} = 0.212) (square), and (T_{c3} = 0.45, $p_{z,c3}$ = 2.235, ρ_{c3} = 0.321) (diamond).The points I, II, III, IV, V, VI, VII, VIII, IX, and X illustrate the coexistence densities at T = 0.075, namely, ρ_{I} = 0.1493, ρ_{II} = 0.1687, ρ_{III} = 0.18562, ρ_{IV} = 0.228, ρ_{V} = 0.2566, and ρ_{VI} = 0.377; at T = 0.175, ρ_{VII} = 0.265; at T = 0.150, $\rho_{0.374}$ = *xxx*; and at T = 0.350, ρ_{IX} = 0.277 and ρ_{X} = 0.364.

continuously, no phase transition at the wall is observed. For rigid nanopores, however, the pressure versus density is a monotonic function for isochores above T_{c3} = 0.45. Below this temperature, a nonmonotonic behavior is observed. The isotherms for $T < T_{ci}$ show a van der Waals loop, characteristic of a first-order phase transition.

For fluids confined inside flexible nanopores the pressure derivative with respect to density is always positive, as illustrated by Figure 4A. For rigid confinement, the derivative is positive only for isochores $T > T_{c3}$. Below this threshold, the function becomes negative for various densities, as illustrated in Figure 4B. This Figure identifies three first -order phase transitions. The densities of the coexistence phases can be obtained by Maxwell construction. These three coexistence regions end in three critical points that can be located by computing the second derivative $d^2p/d\rho^2 = 0$. The coexisting phases and the three critical points are illustrated by symbols in the isochores in Figure 5.

Before discussing the characteristics of the fluid and of the phase transition at the wall, we address the question of why the thermodynamical behavior of flexible nanopores should be different from the case of rigid nanopores. In the rigid case, the walls contribute only to the enthalpic part of the free energy, while in the flexible case, the walls vibrations constantly shake the fluid particles near the wall, also increasing the entropic part of the free energy. While the minimization of the wall−particle and particle−particle energy leads to an ordered structure, the entropic contribution from the wall disrupts this organization. Therefore, only in the case of rigid walls an ordered structure at the wall should be expected. Consequently, because the central layers are not affected by the wall movement, we can understand the differences between the thermodynamical behavior of the confined fluid within rigid and flexible walls by analyzing the properties of the layers in contact with the walls. We will refer to this layer as the contact layer.

Let us first analyze the fluid confined within rigid walls. It is important to remember that the density changes just with the values of L_z because the number of particles and the simulation box size were kept fixed. The fluid within the walls form layers, and as the density decreases (or as the L_z increases) the number of layers increases. Because particles minimize the potential energy by forming layers with $r_z \approx 2\sigma$, as L_z decreases (density increases) the number of layers decreases. Figure 6A illustrates that for T = 0.075 and pressure p_z = 0.762 the system can have five or four layers, and the density would be ρ_{I} =

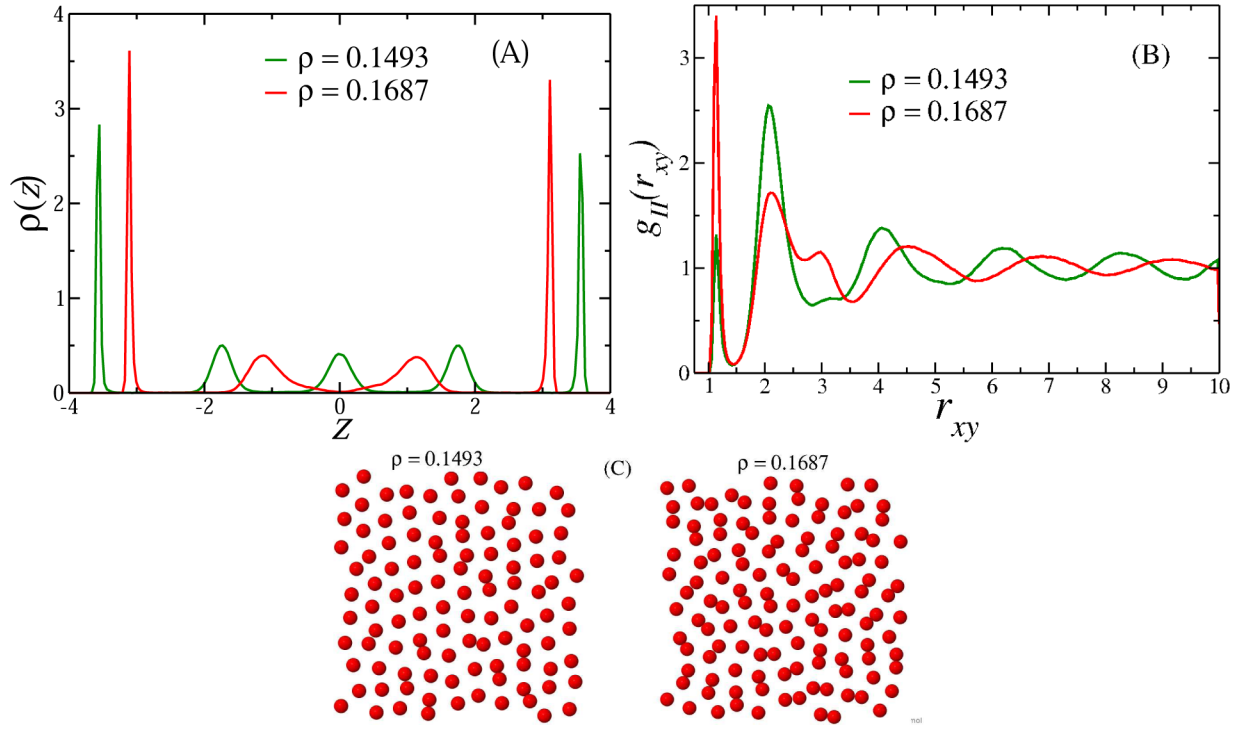

Figure 6. Density histogram (A), radial distribution function (B), and snapshots (C) for the anomalous fluid confined inside a rigid nanopore at T = 0.075 and in the points I and II from Figure 5

dx.doi.org/10.1021/jp5010506 | J. Phys. Chem. C 2014, 118, 9497−9506

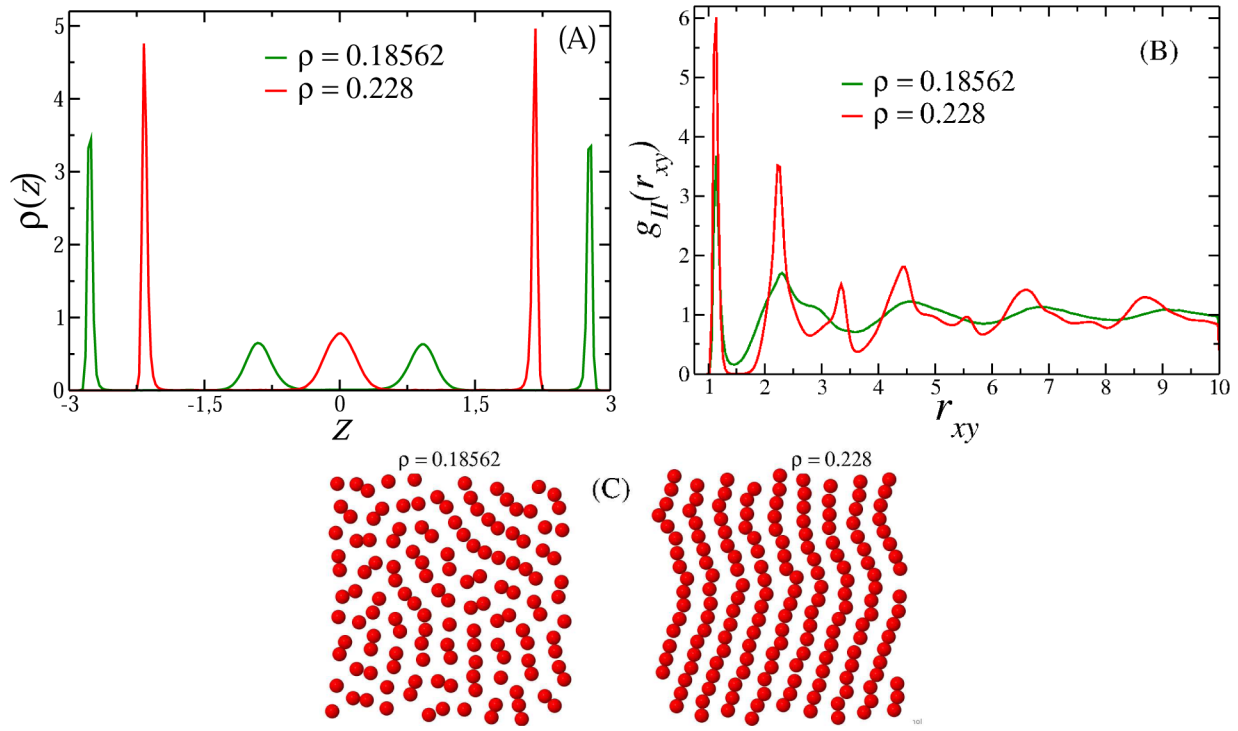

Figure 7. Density histogram (A), radial distribution function (B), and snapshots (C) for the anomalous fluid confined inside a rigid nanopore at T = 0.075 and in the points III and IV from Figure 5

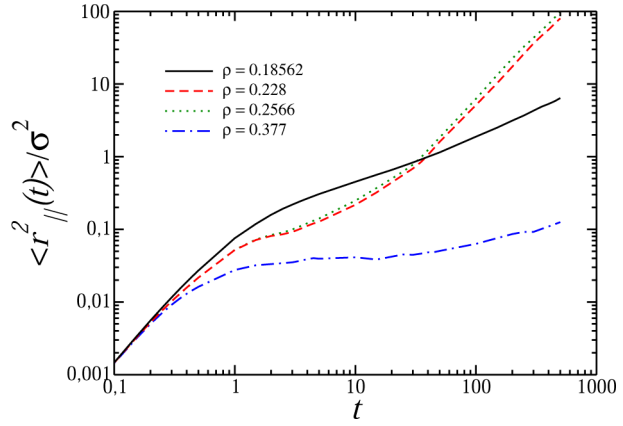

Figure 8. Mean-square displacement in parallel direction as a function of time for the densities of the points III, IV, V, and VI.

0.1493 or ρ_{II} = 0.1687, respectively. Figure 7A shows that the system can have four or three layers at the same temperature and perpendicular pressure if the density would be ρ_{III} = 0.18562 or ρ_{IV} = 0.228, respectively. Finally, Figure 9A has the system with three or two layers depending on if the density would be ρ_V = 0.2566 or ρ_{VI} = 0.377, respectively, with the same value of p_z. These three coexisting regions at T = 0.075 are illustrated in the temperature versus density phase diagram of Figure 5 as I, II, III, IV, V, and VI.

The phase transition observed in Figure 5 can be associated with the change in the number of layers. To explore the idea that this transition is also associated with changes in the structure of the contact layer, we computed the radial distribution function $g_{||}(r_{xy})$ of the contact layer. Figure 6B indicates that for T = 0.075, p_z = 0.762, and the densities ρ_I or ρ_{II} the contact layers exhibit two distinct structures. The high peak in the second length scale for the $g_{||}(r_{xy})$ of ρ_I = 0.1493 and the fact that between the two first peaks the radial distribution function is not equal to zero indicates that this layers is in structured liquid-like state. The $g_{||}(r_{xy})$ for the density ρ_{II} = 0.1687 shows a very structured liquid as well. It has a higher first peak when compared with the peak in the case ρ_I. The ρ_{II} also has a displacement in the subsequent peaks, which suggests an additional length scale in the arrangements of the particles. These two distinct particle arrangement are illustrated in the snapshots of the contact layer shown in Figure 6C. These pictures confirm the two structures predicted by the radial distribution function. The dimeric arrangement corresponds to the increase in the first peak of the $g_{||}(r_{xy})$ for ρ_{II} while the displacement of the other peaks represent the second length. The systems exhibit a first-order phase transition from liquid-crystal like to a dimeric structured liquid in the contact layer.

The $g_{||}(r_{xy})$ for the densities ρ_{III} = 0.18562 and ρ_{IV} = 0.228, associated with the four to three layers in Figure 7A, respectively, are shown in Figure 7B. As the density changes from ρ_{II} to ρ_{III}, the dimeric system becomes continuously more structured. As the density increases further, at ρ_{IV}, the system changes discontinuously to an very ordered liquid structure, characterizing a crystal- or a crystal−liquid-like phase. As the snapshots in Figure 7C indicates, the dimers observed in Figure 6C are now forming ordered lines in the density ρ_{IV}. To clarify if the phase IV is crystal- or liquid-crystal-like phase, the MSD in parallel direction ($r_{||}(t)$) as a function of time on logarithmic scales was computed. Figure 8 shows that despite the high ordering observed in the lining arrangement, phase IV has mobility and therefore is liquid-crystal-like. This result is consistent with other lining phases, and the nature of the phase can be determined by the shear module[75−77] or by the MSD[65] in the nonconfined directions.

dx.doi.org/10.1021/jp5010506 | J. Phys. Chem. C 2014, 118, 9497−9506

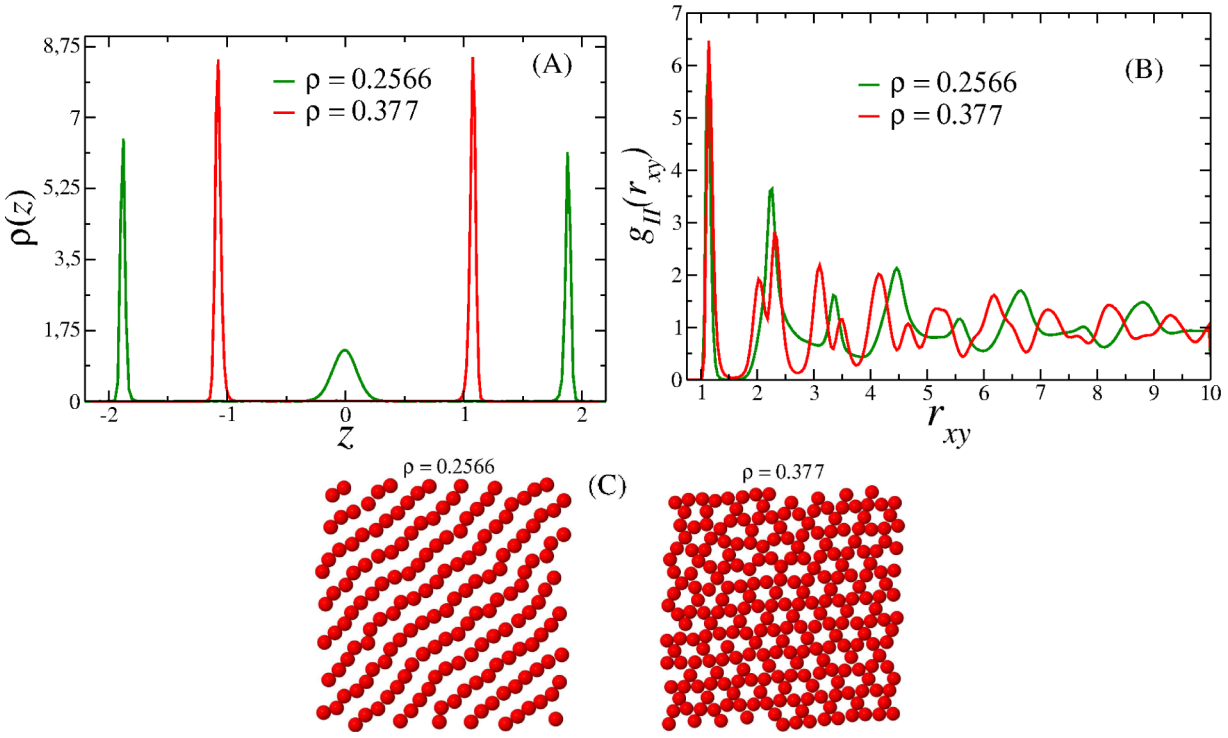

Figure 9. Density histogram (A), radial distribution function (B), and snapshots (C) for the anomalous fluid confined inside a rigid nanopore at T = 0.075 and in the points V and VI from Figure 5

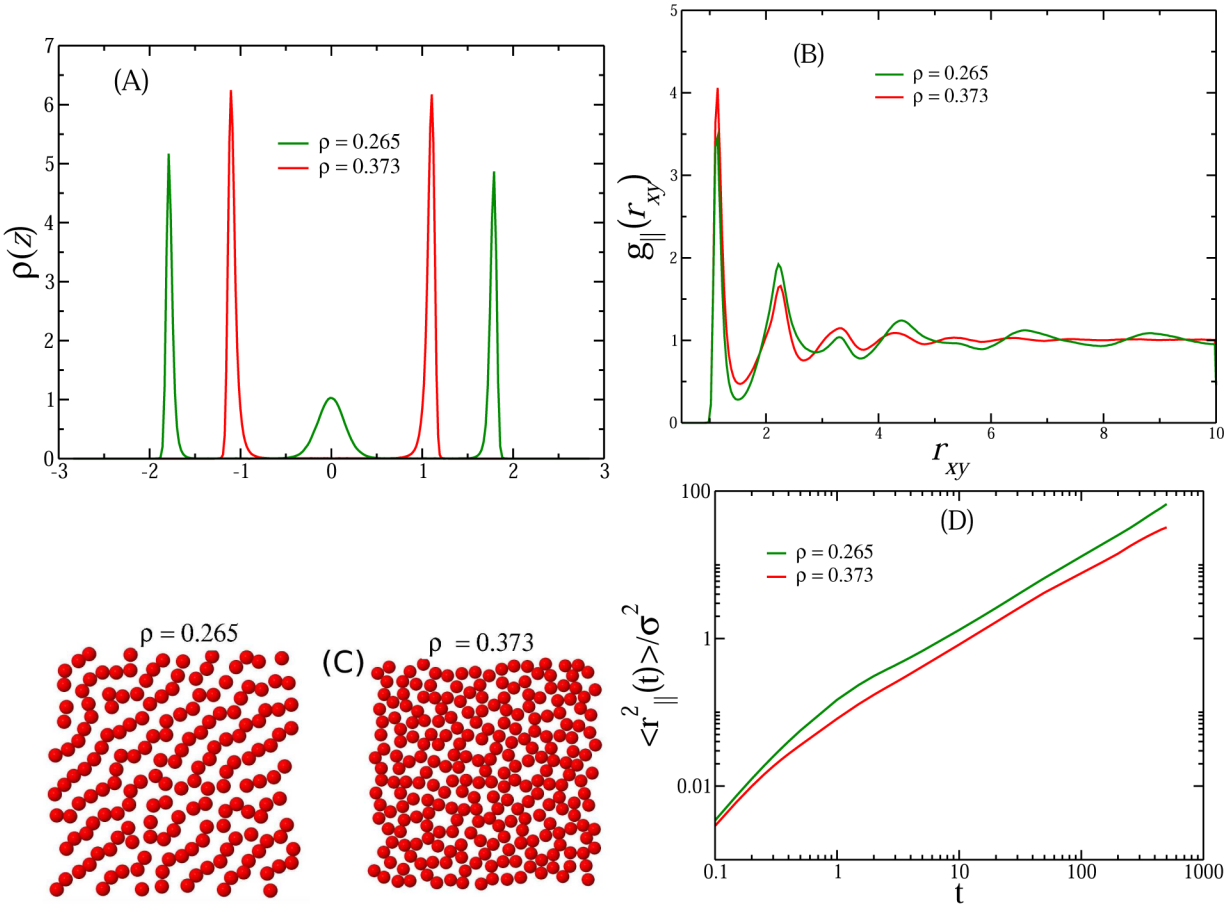

Figure 10. Density histogram (A), radial distribution function (B), snapshots (C), and mean-square displacement (D) for the anomalous fluid confined inside a rigid nanopore at T = 0.175 and in the points VII and VIII from Figure 5

dx.doi.org/10.1021/jp5010506 | J. Phys. Chem. C 2014, 118, 9497−9506

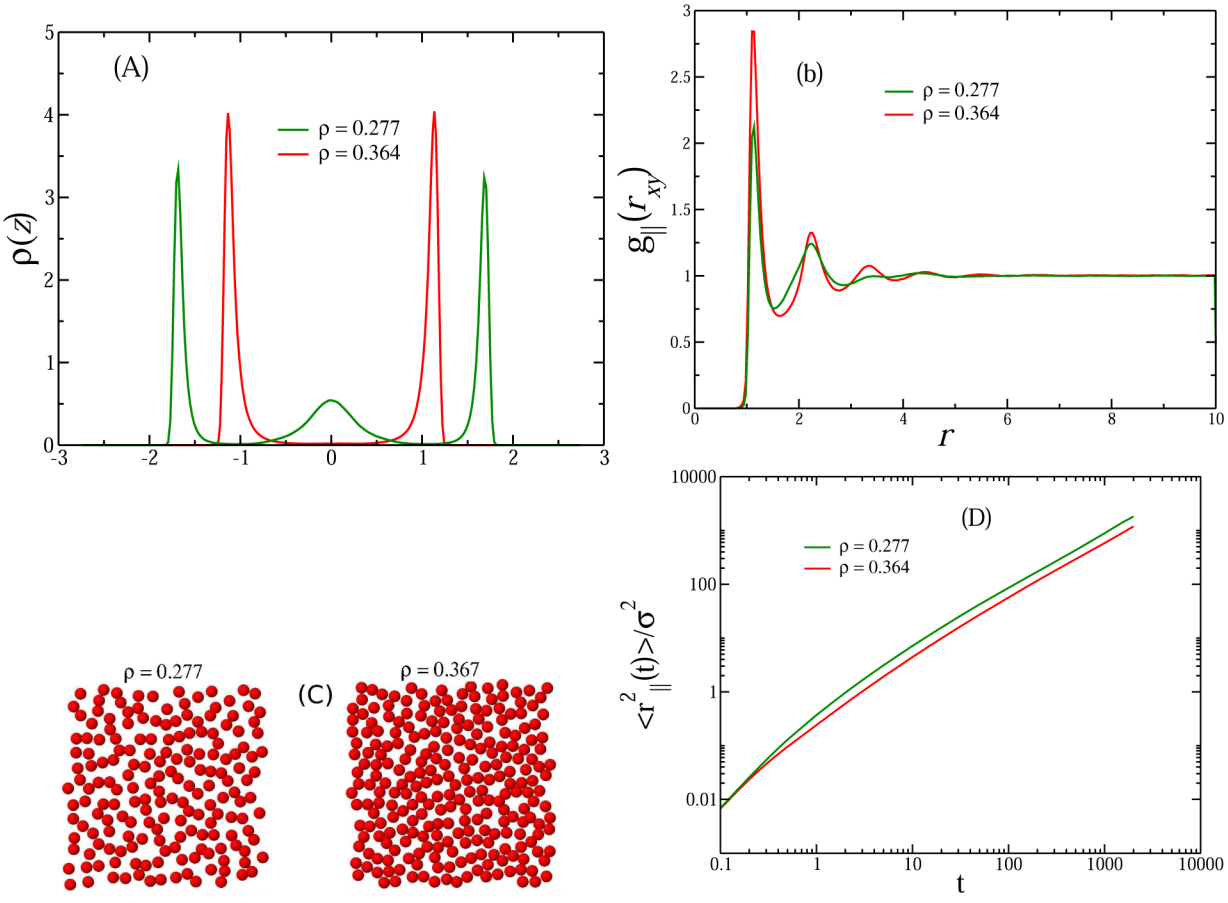

Figure 11. Density histogram (A), radial distribution function (B), snapshots (C), and mean-square displacement (D) for the anomalous fluid confined inside a rigid nanopore at T = 0.350 and in the points IX and X from Figure 5.

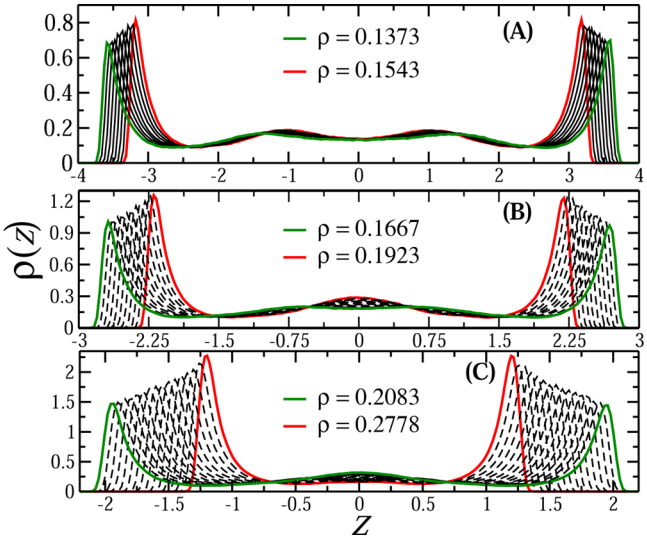

Figure 12. Density histogram for the anomalous fluid confined inside a rigid nanopore at temperatures above the critical point, T = 1.0.

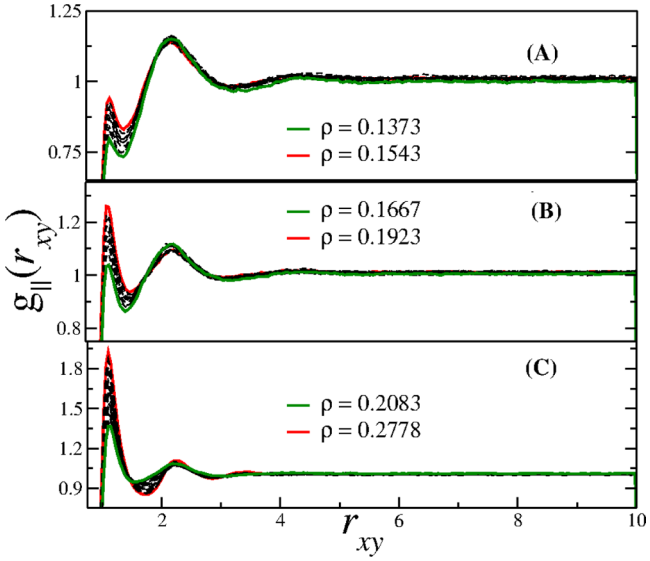

Figure 13. $g_{\|}(r_{xy})$ for the anomalous fluid confined inside a rigid nanopore at temperatures above the critical point, T = 1.0.

The radial distribution functions for densities ρ_V = 0.2566 and ρ_{VI} = 0.377 illustrated in Figure 9B show a coexistence of two different highly ordered structures in the contact layer: a liquid-crystal and a solid phase. Analysis using the snapshot of Figure 9C shows that for ρ_V the particles form lines that can be in different orientations. The snapshots show a structural transition from the lined conformation to a honeycomb structure. This result indicates that the third van der Waals loop at low temperature corresponds to a liquid-crystal-solid phase transition in the contact layer. To confirm the liquid-crystal behavior, we plot in Figure 8 the MSD in parallel direction ($r_{\|}(t)$) as a function of time on logarithmic scales. The diffusion of ρ_V = 0.2566 is larger in relation to liquid phase (ρ_{III}

dx.doi.org/10.1021/jp5010506 | J. Phys. Chem. C 2014, 118, 9497−9506

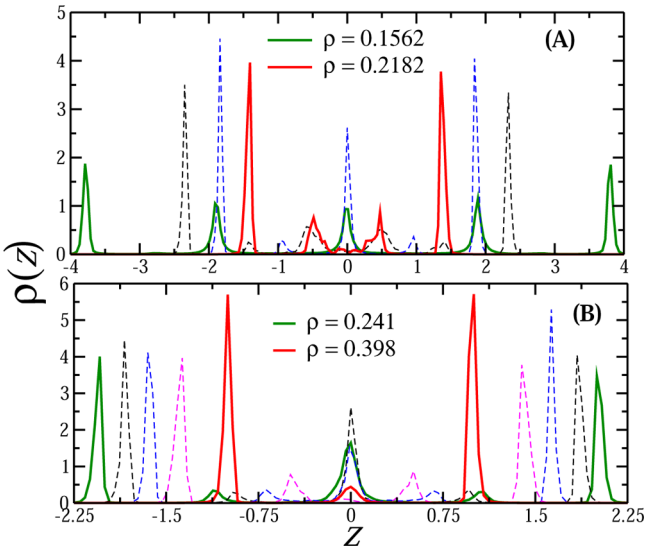

Figure 14. Density histogram (left, panels A and B) and $g_{\parallel}(r_{xy})$ (right, panels C and D) for the anomalous fluid confined inside a flexible nanopore at a low temperature, T = 0.10.

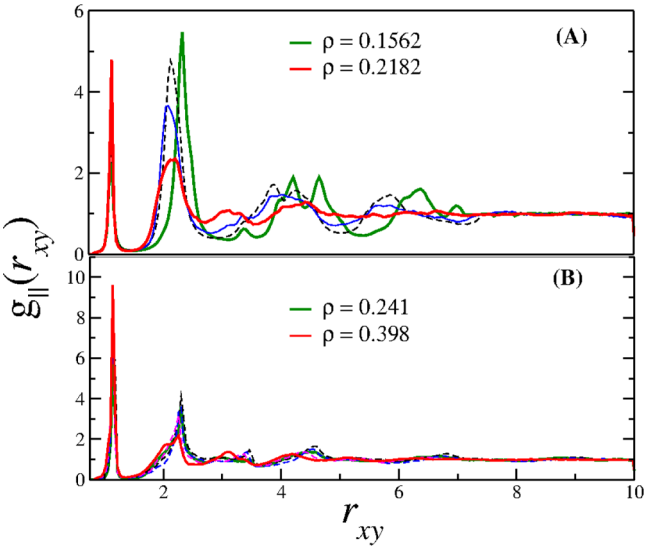

Figure 15. $g_{\parallel}(r_{xy})$ (right, panels C and D) for the anomalous fluid confined inside a flexible nanopore at a low temperature, T = 0.10.

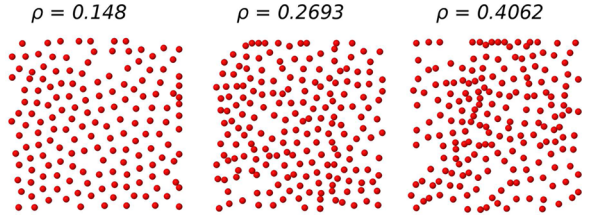

Figure 16. Contact layer snapshots in the flexible nanopore case. In all cases, a fluid-like structure was observed.

= 0.18562) and to the solid honeycomb phase (ρ_{VI} = 0.377). So, the densities ρ_{IV} and ρ_{V} present a very ordered configuration but with a high mobility.

The three phase transitions at the surface are represented by the density jumps in the temperature versus density phase transition in Figure 5 and by the van der Waals loops in Figure 3, showing that the instabilities signalized in these graphs are

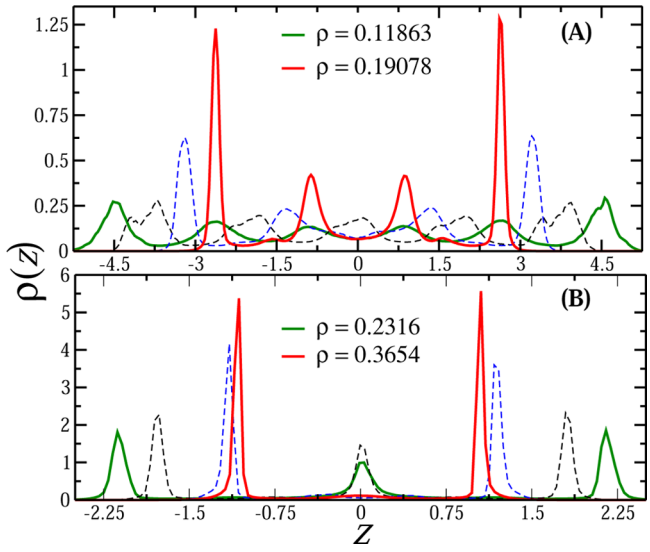

Figure 17. Density histogram for the anomalous fluid confined inside a flexible nanopore at a elevated temperature, T = 1.0.

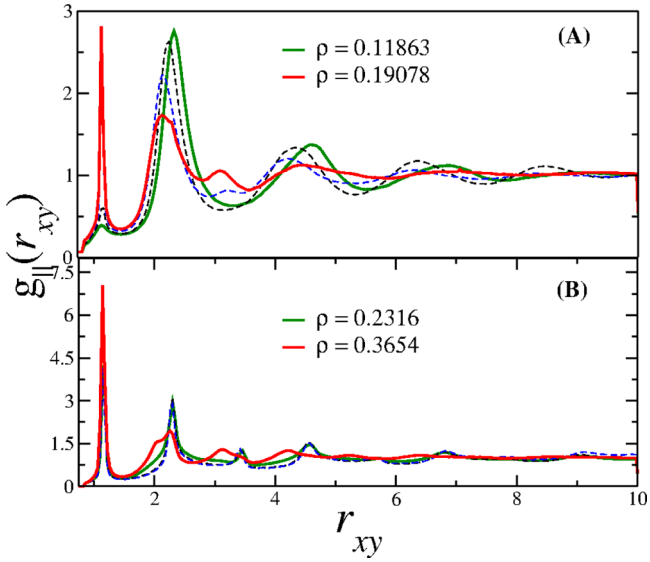

Figure 18. $g_{\parallel}(r_{xy})$ for the anomalous fluid confined inside a flexible nanopore at a elevated temperature, T = 1.0.

related to phase transitions at the fluid wall interface. The transition between a liquid-crystal and solid phases usually implies a change in the order parameter symmetry and therefore cannot be modeled by a van der Waals theory. However, Daanoun, Tejero, and Baus showed that the van der Waals theory can be extended to transitions between structured phases[78] in some special cases.

To reconcile the transition between a liquid-crystal-like to solid transition with the presence of a critical point, we analyzed two different sets of temperatures. First, the density histogram, the radial distribution function, the MSD, and the snapshot of densities ρ_{VII} and ρ_{VIII} were computed for T = 0.175. Figure 10 shows that phase VII is more structured when compared with phase V and is quite mobile, while phase VIII is less structured than phase VI and the MSD is also higher when compared with phase VI. This suggests that phase VIII has some resemblance with the hexactic phase.[79] Next, for T = 0.350, the density histogram, the radial distribution function, the MSD, and the

dx.doi.org/10.1021/jp5010506 | J. Phys. Chem. C 2014, 118, 9497−9506

snapshot of densities ρ_{IX} and ρ_{X} were computed. Figure 11 indicates that phases IX and X are liquid. Therefore, the critical point (T_{c3} = 0.45, $p_{z,c3}$ = 2.235) is between two liquid phases.

For temperatures above the critical region the number of layers of the anomalous fluid confined inside a rigid nanopore does not change significantly. Figure 12A−C illustrates the density across the nanopore for various plates separation, showing two contact layers and a uniform distribution inside the pore. The radial distribution function of the contact layer, presented in Figure 13A−C, shows a fluid-like behavior for all densities. In this way, at high temperatures the layers transition does not occur and the structure of the contact layer does not change, and no phase transition is observed.

Next, we analyze the behavior of the anomalous fluid inside a flexible nanopore. Figure 14A,B shows the number of layers for different densities at T = 0.10. As the density is increased, the number of layers decrease from five to two layers. The nanopore flexibility also leads to a distinct behavior in the contact layer structure, which is strongly affected by the walls movement. Figure 15A,B illustrates the radial distribution function of the contact layer for various densities. In all cases the $g_{ll}(r_{xy})$ shows a distinct signature of amorphous phase. This observation is supported by the snapshot shown in Figure 16. The system exhibits a disordered structure similar to the amorphous phase. No phase transition is present, as already indicated by Figure 4A.

It is important to point out that the wall flexibility, despite maintaining the contact layer in a disordered structure, makes it more difficult to destroy the central layers at higher temperatures. At right temperatures, such as T = 1.0, and small density the system shows a bulk-like density profile, as shown in Figure 17A, but for slightly higher densities, layering of the fluid is restored as illustrated in Figure 17B. This behavior is distinct from the rigid nanopore case in which for any density at high temperatures the layering is lost. Because of the wall oscillations, the fluid particles can assume in the z direction a position that minimizes the energy, and this small oscillation, compared with fixed walls, leads to the layering even for high temperatures, as shown in Figure 17A,B. This order in the middle layers at high temperatures does not affect the contact layer. Figure 18A,B shows that the radial distribution function of the contact layer is similar to the amorphous phase.

4. CONCLUSIONS

We have studied the thermodynamical behavior and the surface phase transition of a anomalous fluid confined inside rigid and flexible nanopores. Our results show that the fluid behavior is strongly affected by the confinement properties. In the rigid nanopore scenario, the $p_z \times \rho$ phase diagram shows the presence of three first-order phase transitions related to structural phase transitions at the contact layer. Because of the walls fluctuations in the flexible nanopore case, no surface phase transition is observed in the case of nonrigid walls. Our results indicate that the thermodynamic behavior of anomalous fluids such as water obtained for rigid carbon nanotubes and solid state nanopores cannot be extrapolated to more flexible walls such as the surface present in biological systems.

AUTHOR INFORMATION

Corresponding Authors

*E-mail: josebordin@unipampa.edu.br.
*E-mail: leandro.krott@ufrgs.br.
*E-mail: marciabarbosa@ufrgs.br.

Notes

The authors declare no competing financial interest.

ACKNOWLEDGMENTS

J.R.B. thanks Prof. A. Diehl from UFPel for the discussions. We thank the Brazilian agencies CNPq, INCT-FCx, and Capes for the financial support. We also thank CEFIC - Centro de Física Computacional of Physics Institute at UFRGS and the TSSC - Grupo de Teoria e Simulação em Sistemas Complexos at UFPel for the computer clusters.

REFERENCES

(1) Chaplin, M. *Sixty-Nine Anomalies of Water*. http://www.lsbu.ac.uk/water/anmlies.html, 2013.
(2) Kell, G. S. *J. Chem. Eng. Data* **1975**, *20*, 97.
(3) Angell, C. A.; Finch, E. D.; Bach, P. *J. Chem. Phys.* **1976**, *65*, 3065.
(4) Prielmeier, F. X.; Lang, E. W.; Speedy, R. J.; Lüudemann, H.-D. *Phys. Rev. Lett.* **1987**, *59*, 1128.
(5) Thurn, H.; Ruska, J. *J. Non-Cryst. Solids* **1976**, *22*, 331.
(6) *Handbook of Chemistry and Physics*, 65th ed.; CRC Press: Boca Raton, FL, 1984.
(7) Sauer, G. E.; Borst, L. B. *Science* **1967**, *158*, 1567.
(8) Kennedy, S. J.; Wheeler, J. C. *J. Chem. Phys.* **1983**, *78*, 1523.
(9) Tsuchiya, T. *J. Phys. Soc. Jpn.* **1991**, *60*, 227.
(10) Cummings, P. T.; Stell, G. *Mol. Phys.* **1981**, *43*, 1267.
(11) Togaya, M. *Phys. Rev. Lett.* **1997**, *79*, 2474.
(12) Angell, C. A.; Bressel, R. D.; Hemmatti, M.; Sare, E. J.; Tucker, J. C. *Phys. Chem. Chem. Phys.* **2000**, *2*, 1559.
(13) Shell, M. S.; Debenedetti, P. G.; Panagiotopoulos, A. Z. *Phys. Rev. E* **2002**, *66*, 011202.
(14) Sharma, R.; Chakraborty, S. N.; Chakravarty, C. *J. Chem. Phys.* **2006**, *125*, 204501.
(15) Sastry, S.; Angell, C. A. *Nat. Mater.* **2003**, *2*, 739.
(16) Chen, S.-H.; Mallamace, F.; Mou, C.-Y.; Broccio, M.; Corsaro, C.; Faraone, A.; Liu, L. *Proc. Natl. Acad. Sci. U.S.A.* **2006**, *103*, 12974.
(17) Morishita, T. *Phys. Rev. E* **2005**, *72*, 021201.
(18) Netz, P. A.; Starr, F. W.; Stanley, H. E.; Barbosa, M. C. *J. Chem. Phys.* **2001**, *115*, 344.
(19) Netz, P. A.; Starr, F. W.; Barbosa, M. C.; Stanley, H. E. *Physica A* **2002**, *314*, 470.
(20) Berendsen, H. J. C.; Grigera, J. R.; Straatsma, T. P. *J. Phys. Chem.* **1987**, *91*, 6269.
(21) Abascal, J. L. F.; Vega, C. *J. Chem. Phys.* **2005**, *123*, 234505.
(22) Mahoney, M. W.; Jorgensen, W. L. *J. Chem. Phys.* **2000**, *112*, 8910.
(23) Stillinger, F. H.; Weber, T. A. *Phs. Rev. B* **1985**, *31*, 5262.
(24) van Beest, B.; Kramer, G.; van Santen, R. *Phs. Rev. Lett.* **1990**, *64*, 1955.
(25) Jagla, E. A. *Phys. Rev. E* **1998**, *58*, 1478.
(26) Xu, L.; Buldyrev, S.; Angell, C. A.; Stanley, H. E. *Phys. Rev. E* **2006**, *74*, 031108.
(27) Yan, Z.; Buldyrev, S. V.; Giovambattista, N.; Stanley, H. E. *Phys. Rev. Lett.* **2005**, *95*, 130604.
(28) Xu, L.; Kumar, P.; Buldyrev, S. V.; Chen, S.-H.; Poole, P.; Sciortino, F.; Stanley, H. E. *Proc. Natl. Acad. Sci. U.S.A.* **2005**, *102*, 16558.
(29) de Oliveira, A. B.; Netz, P. A.; Colla, T.; Barbosa, M. C. *J. Chem. Phys.* **2006**, *124*, 084505.
(30) Camp, P. *Phys. Rev. E* **2005**, *71*, 031507.
(31) Wilding, N. B.; Magee, J. E. *Phys. Rev. E* **2002**, *66*, 031509.
(32) Almarza, N. G.; Capitan, J. A.; Cuesta, J. A.; Lomba, E. *J. Chem. Phys.* **2009**, *131*, 124506.
(33) Fomin, D. Y.; Gribova, N. V.; Ryzhov, V. N.; Stishov, S. M.; Frenkel, D. *J. Chem. Phys.* **2008**, *129*, 064512.
(34) Franzese, G.; Malescio, G.; Skibinsky, A.; Buldyrev, S. V.; Stanley, H. E. *Nature (London)* **2001**, *409*, 692.
(35) Franzese, G.; Stanley, H. E. *J. Phys.: Condens. Matter* **2007**, *19*, 205126.

(36) de Oliveira, A. B.; Netz, P. A.; Colla, T.; Barbosa, M. C. *J. Chem. Phys.* **2006**, *125*, 124503.
(37) Jr, N. M. B.; Salcedo, E.; Barbosa, M. C. *J. Chem. Phys.* **2009**, *131*, 094504.
(38) da Silva, J. N.; Salcedo, E.; de Oliveira, A. B.; Barbosa, M. C. *J. Chem. Phys.* **2010**, *133*, 244506.
(39) Malescio, G.; Franzese, G.; Skibinsky, A.; Buldyrev, S. V.; Stanley, H. E. *Phys. Rev. E* **2005**, *71*, 061504.
(40) Holt, J. K.; Park, H. G.; Wang, Y. M.; Stadermann, M.; Artyukhin, A. B.; Grigoropulos, C. P.; Noy, A.; Bakajin, O. *Science* **2006**, *312*, 1034.
(41) Whitby, M.; Cagnon, L.; N. Quirke, M. T. *Nano Lett.* **2008**, *8*, 2632.
(42) Cui, S. T.; Cummings, P. T.; Cochran, H. D. *J. Chem. Phys.* **2001**, *114*, 7189.
(43) Jabbarzadeh, A.; Harrowell, P.; Tanner, R. I. *J. Chem. Phys.* **2006**, *125*, 034703.
(44) Jakobtorweihen, S.; Verbeek, M. G.; Lowe, C. P.; Keil, F. J.; Smit, B. *Phys. Rev. Lett.* **2005**, *95*, 044501.
(45) Chen, H.; Johnson, J. K.; Sholl, D. S. *J. Phys. Chem. B* **2006**, *110*, 1971−1975.
(46) Qin, X.; Yuan, Q.; Zhao, Y.; Xie, S.; Liu, Z. *Nano Lett.* **2011**, *11*, 2173.
(47) Erko, M.; Cade, N.; Michette, A. G.; Findenegg, G. H.; Paris, O. *Phys. Rev. B* **2011**, *84*, 104205.
(48) Deschamps, J.; Audonnet, F.; Brodie-Linder, N.; Schoeffel, M.; Alba-Simionesco, C. *Phys. Chem. Chem. Phys.* **2010**, *12*, 1440.
(49) Jähnert, S.; Chávez, F. V.; Schaumann, G. E.; Schreiber, A.; Schönhoff, M.; Findenegg, G. H. *Phys. Chem. Chem. Phys.* **2008**, *10*, 6039.
(50) Morishige, K.; Nobuoka, K. *J. Chem. Phys.* **1997**, *107*, 6965.
(51) Kastelowitz, N.; Johnston, J. C.; Molinero, V. *J. Chem. Phys.* **2010**, *132*, 124511.
(52) Mao, Z.; Sinnot, S. B. *Phys. Rev. Lett.* **2002**, *89*, 278301.
(53) Ackerman, D. M.; Skoulidas, A. I.; Sholl, D. S.; Johnson, J. K. *Mol. Simul.* **2003**, *29*, 677.
(54) Khademi, M.; Sahimi, M. *J. Chem. Phys.* **2011**, *135*, 204509.
(55) Lee, K. P.; Leese, H.; Mattia, D. *Nanoscale* **2012**, *4*, 2621.
(56) Giovambattista, N.; Rossky, P. J.; Debenedetti, P. G. *Phys. Rev. Lett.* **2009**, *102*, 050603.
(57) Lombardo, T. G.; Rossky, P. J.; Debenedetti, P. G. *Faraday Discuss.* **2009**, *141*, 359.
(58) Koga, K.; Gao, G. T.; Tanaka, H.; Zeng, X. C. *Nature* **2001**, *412*, 802−805.
(59) Noskov, S. Y.; Berneche, S.; Roux, B. *Nature* **2004**, *431*, 830.
(60) Beckstein, O.; Sansom, M. S. P. *Phys. Biol.* **2004**, *1*, 42.
(61) Allen, T. W.; Andersen, O. S.; Roux, B. *J. Gen. Physiol.* **2004**, *124*, 679.
(62) Chiu, S.-W.; Jakobsson, E.; Subramahiam, S.; McCammon, J. A. *Biophys. J.* **1991**, *60*, 273.
(63) Krott, L.; Bordin, J. R. *J. Chem. Phys.* **2013**, *139*, 154502.
(64) Krott, L.; Barbosa, M. C. *J. Chem. Phys.* **2013**, *138*, 084505.
(65) Krott, L.; Barbosa, M. C. *Phys. Rev. E* **2014**, *89*, 012110.
(66) Bordin, J. R.; de Oliveira, A. B.; Diehl, A.; Barbosa, M. C. *J. Chem. Phys.* **2012**, *137*, 084504.
(67) Bordin, J. R.; Diehl, A.; Barbosa, M. C. *J. Phys. Chem. B* **2013**, *117*, 7047−7056.
(68) Allen, P.; Tildesley, D. J. *Computer Simulation of Liquids*; Oxford University Press: Oxford, U.K., 1987.
(69) de Oliveira, A. B.; Salcedo, E.; Chakravarty, C.; Barbosa, M. C. *J. Chem. Phys.* **2010**, *132*, 234509.
(70) Weeks, J. D.; Chandler, D.; Andersen, H. C. *J. Chem. Phys.* **1971**, *54*, 5237.
(71) Zangi, R.; Rice, A. *Phys. Rev. E* **2000**, *61*, 660.
(72) Lupowski, M.; van Smol, F. *J. Chem. Phys.* **1990**, *93*, 737.
(73) Kumar, P.; Buldyrev, S. V.; Sciortino, F.; Zaccarelli, E.; Stanley, H. E. *Phys. Rev. E* **2005**, *72*, 021501.
(74) Kumar, P.; Starr, F. W.; Buldyrev, S. V.; Stanley, H. E. *Phys. Rev. E* **2007**, *72*, 011202.
(75) Camp, P. J. *Phys. Rev. E* **2003**, *68*, 061506.
(76) Camp, P. J. *Phys. Rev. E* **2005**, *71*, 031507.
(77) de Oliveira, A. B.; Nevez, E.; Gavazzoni, C.; Paukowski, J. Z.; Netz, P. A.; Barbosa, M. C. *J. Chem. Phys.* **2010**, *132*, 164505.
(78) Daanoun, A.; Tejero, C. F.; Baus, M. *Phys. Rev. E* **1994**, *40*, 2913.
(79) Dudalov, D.; Fomin, Y. D.; Tsiok, E.; Ryzhov, V. arXiv:1311.7534v1 [cond-mat.soft], 2013.